Single and Multiple Pulse Pattern Formation in All-Normal All-PM Yb-Doped Fiber Laser Using a Nonlinear Optical Loop Mirror

Luqi Guo, Zebiao Gan, and Xiaoyan Liang

***Abstract*—We report the evolution of single-pulse and multi-pulse in a mode-locked all polarization-maintaining fiber laser based on a nonlinear optical loop mirror (NOLM). The main parameters of the laser were determined by numerically simulating the relationship between the number of pulses and the basic parameters of each element. Experiments demonstrate generation of 1 to 6 pulses per cavity round trip. There is an unstable regime between the stable N and N + 1 pulses states when gradually increasing the pump power, while the intervals of the unstable regime shrink or even disappear when the direction of pump power variation is reversed. Our experimental results are different from those previously reported where the intervals of the unstable pulse regime are almost unchanged regardless of the pump power adjustment direction. We also describe how to obtain fundamental mode-locking from the multi-pulse state. The laser operated in the single-pulse regime shows excellent stability.**

***Index Terms*—Mode-locked fiber laser, nonlinear optical loop mirror, dissipative solitons, multiple pulsing.**

I. Introduction

ULTRAFAST mode-locked fiber lasers in particular which operated in the 1 μm range have attracted widespread attention in many fields [1], [2], [3] because of their higher output pulse energy, compact structure, cost-effectiveness and excellent stability. Material saturable absorbers are often adopted in the femtosecond fiber lasers. However, they suffer from a relatively low damage threshold and a tendency to degrade over time. Nonlinear polarization evolution (NPE) is one of the most common artificial saturable absorber mechanisms used to achieve pulsed operation in fiber lasers [4], [5], [6]. But conventional NPE systems based on non-polarization maintaining (PM) fibers tend to be very sensitive to environmental changes. Another approach to designing an environmentally stable all-PM-fiber mode-locked laser relies on nonlinear optical fiber loop mirrors (NOLM) or nonlinear amplifying fiber loop mirrors (NALM) as an artificial saturable absorber. NALM is modified by adding an amplifying stage inside the NOLM loop, allowing better control and easier self-starting operation [7], [8], [9]. Compared to NPE and NALM, NOLM is the most economical and simplest method to achieve mode-locking in fiber lasers.

Pulses in all normal-dispersion (ANDi) mode-locked fiber lasers can be understood as dissipative solitons (DSs) which can tolerate relatively large pulse energy in a normal dispersion regime as a highly chirped pulse. However, the multi-pulse operation is still inevitable when the pump power is higher than a threshold. The interaction between these pulses serves as an ideal platform for investigating various complex nonlinear dynamics like soliton molecules [10], disordered bunched multi-soliton [11], [12], harmonic mode-locking [13] and soliton rains [14], [15], [16]. It is of great significance to research multiple pulse dynamics in mode-locked fiber lasers. On the one hand, a detailed understanding of their physical mechanism is helpful to further improve the performance of the lasers. On the other hand, the controllable multi-pulse operation of ultrafast fiber lasers is important for various applications. For instance, they can be used to develop extra-high-speed optical communication systems [17], [18], [19], improve the ablation rate in femtosecond laser micromachining [2] and detect weak signals such as space debris [20]. It has been found that in the field of micromachining, multi-pulse laser processing can achieve better results than single-pulse processing [21].

So far, multi-pulsing dynamics have been studied by numerical or/and experimental methods in various types of fiber lasers. Tang et al. found numerically that the formation of multiple solitons in the laser operated in the anomalous dispersion regime is caused by a peak-power-limiting effect of the laser cavity [22]. With the method of nonlinear Fourier transform, Wang et al. demonstrated that resonant continuous wave (CW) always shares intracavity energy with solitons and affects the solitons evolution well with pump power shuttling [23], [24]. In the normal dispersion regime, Haboucha et al. identified the spectral gain filtering as a mechanism of multiple pulse formation [25], and Liu et al. further confirmed this conclusion through numerical and experimental studies [26]. Despite the great amount of work, to the best of our knowledge, no systematic

Manuscript received 6 October 2022; revised 19 November 2022; accepted 30 November 2022. Date of publication 5 December 2022; date of current version 14 December 2022. This work was supported by the National Natural Science Foundation of China under Grant 62005299. *(Corresponding author: Zebiao Gan.)*

Luqi Guo is with the State Key Laboratory of High Field Laser Physics, Shanghai Institute of Optics and Fine Mechanics, Chinese Academy of Sciences, Shanghai 201800, China, also with the University of Chinese Academy of Sciences, Beijing 100049, China, and also with the ShanghaiTech University, Shanghai 201210, China (e-mail: guolq@shanghaitech.edu.cn).

Zebiao Gan and Xiaoyan Liang are with the State Key Laboratory of High Field Laser Physics, Shanghai Institute of Optics and Fine Mechanics, Chinese Academy of Sciences, Shanghai 201800, China (e-mail: gzb@siom.ac.cn; liangxy@siom.ac.cn).

Digital Object Identifier 10.1109/JPHOT.2022.3226513

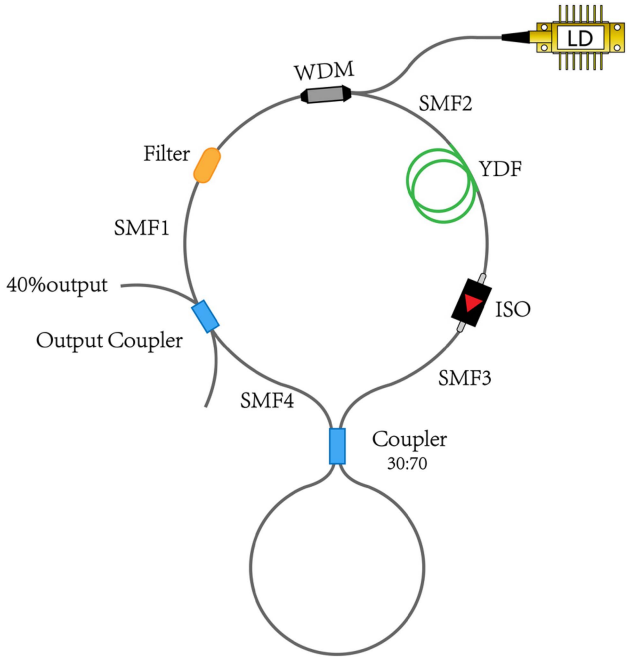

Fig. 1. Schematic of the laser.

experimental study related to the generation of multiple pulses in an all-normal all polarization-maintaining (PM) mode-locked fiber laser based on nonlinear optical fiber loop mirrors (NOLM) have been reported. The first all-PM fiber ANDi oscillator based on NOLM was demonstrated by Szczepanek et al. [27]. In their study, a strong CW component appeared at the maximum available pump power. However, the multi-pulse formation was not observed. Cai et al. numerical studied the characteristics of output pulses from a NOLM-based ANDi fiber laser under different cavity parameters. However, no relevant experiments are given to prove the conclusions of the simulation [28]. Pielach et al. observed the formation of multiple pulses in a mode-locked laser with NOLM [29], however, their research mainly focuses on single pulse operation and there is no detailed description of the multi-pulse state. Moreover, their laser under the multi-pulse mode of operation was unstable.

In this article, we present simulation results to illustrate the influence of various design parameters on the number of mode-locked pulses. Multi-pulse can occur while the filter bandwidth reduces within a certain range. We experimentally study the multi-pulse operation states of a mode-locked all-PM ytterbium-doped (Yb-doped) fiber laser using a NOLM. Generation of 1 to 6 DSs per cavity round trip was demonstrated by adjusting the pump power level. We observed the hysteresis phenomena when the pump power was modified. We also show how to enter a stable single-pulse mode-locked state from a multi-pulse regime.

II. Numerical Simulations

Fig. 1 shows the schematic of the laser model for numerical simulation. The resonator is built in a typical figure-eight configuration and consists of two loops combined by a 2×2 coupler. The NOLM loop is made of a coupler and a piece of PM fiber.

TABLE I
Parameter Range in Simulations

symbol	description	parameter range
SMF1	SMF after random white noise input	2.05m
Filter.BW	Bandwidth of Filter	2/4/6/8/10nm
SMF2	SMF between Filter and YDF	3.22m
Yb.L	Length of Yb-doped fiber	1m
SMF3	SMF after YDF	2.83m
NOLM.L	Length of NOLM	2/3/4/5m
K	Power splitting ratio of fiber coupler	10%/20%/30%/ 40%
SMF4	SMF after NOLM	2.02m
OC	Out coupler	40% output

The main loop of the laser contains a piece of Yb-doped PM fiber which is pumped by a 976 nm laser diode via a wavelength division multiplexer (WDM). After the Yb-doped fiber, an isolator ensures the unidirectional operation of the oscillation. Before the Yb-doped fiber, a bandpass filter is used to ensure the cavity's boundary conditions by reducing the spectral bandwidth of the pulse reinjected into the gain section. In addition, an output coupler is placed in the main loop to extract part of the power in the cavity as an output. All components are connected via polarization maintaining single-mode fiber (SMF) PM980-XP. Table I lists the range of parameters we used in the simulation.

The parametric effects considered in our simulations include filter bandwidth, length of NOLM loop, and coupler power splitting ratio. For each parameter under study, we will keep all other parameters fixed.

Propagation of the complex electric field envelope of the pulse in Yb-doped fiber can be described by using the generalized nonlinear Schrodinger equation (GNLSE) including saturated gain with a finite bandwidth:

$$\frac{\partial \mathrm{A}}{\partial \mathrm{z}}+\frac{\mathrm{g}_0}{2}A+\frac{\mathrm{i}\beta_2}{2}\frac{\partial^2 \mathrm{A}}{\partial \mathrm{T}^2}-\frac{\beta_3}{6}\frac{\partial^3 \mathrm{A}}{\partial \mathrm{T}^3} =\mathrm{i}\gamma\left(1+\mathrm{i}\frac{1}{\omega_0}\frac{\partial}{\partial \mathrm{T}}\right)\left(\mathrm{A}\left(\mathrm{z},\mathrm{T}\right)\int_0^\infty \mathrm{R}\left(\mathrm{t}'\right)\left|\mathrm{A}\left(\mathrm{z},\mathrm{T}-\mathrm{t}'\right)\right|^2 \mathrm{dt}'\right) \tag{1}$$

Where A is the amplitude of the optical pulse envelope; β_2 and β_3 are the group velocity dispersion and third-order dispersion; γ is the nonlinearity coefficient; z is the propagation distance; T is the retarded time; R(t) is the nonlinear response; and g_0 is the spectrum-dependent net gain coefficient:

$$\mathrm{g}_0=\frac{\mathrm{g}_{\mathrm{ss}}}{1+\mathrm{P}_{\mathrm{av}}/\mathrm{P}_{\mathrm{sat}}}\cdot \mathrm{g}\left(\omega\right) \tag{2}$$

Where gss is the small signal gain coefficient at the wavelength corresponding to the peak gain. Since the small signal gain coefficient is proportional to the pumping strength, increasing gss corresponds to increasing the pump power in the experiments. For passive fiber, gss = 0. In our simulation, $\mathrm{g}(\omega)$

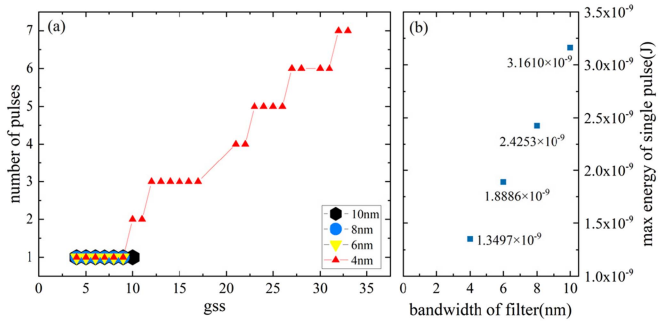

Fig. 2. Laser maximum output energy and pulse count with respect to the bandwidth of filter. (a) Relationship between bandwidth of filter and number of pulses. (b) Relationship between bandwidth of filter and maximum energy of single pulse.

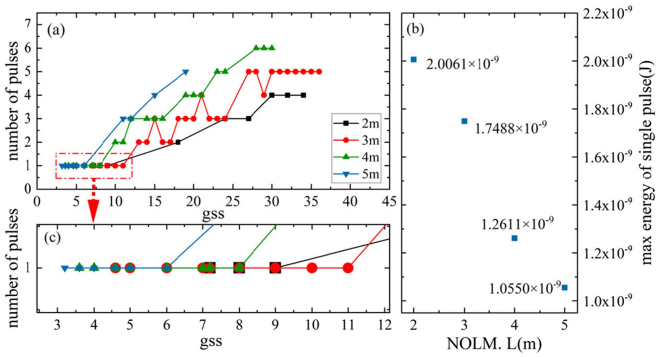

Fig. 3. Laser maximum output energy and pulse count with respect to length of NOLM loop. (a) Relationship between length of NOLM and number of pulses. (b) Relationship between length of NOLM loop and maximum energy of single pulse.

is a normalized Lorentzian gain shape function with 30 nm bandwidth; Pav is average power and Psat is saturation power which can be calculated according to

$$\mathrm{P_{sat}} = \frac{\mathrm{Sh}\nu}{(\sigma_{\mathrm{em}} + \sigma_{\mathrm{abs}})\,\tau} \tag{3}$$

Where S is effective mode field area; σ_{em} and σ_{abs} are emission cross section and absorption cross section at the emission wavelength; and τ is upper level lifetime.

To simulate NOLM [9], we first divide the input light field ($\mathrm{A_{in}}$) into clockwise (A_c) and anticlockwise ($\mathrm{A_{ac}}$) propagating fields as $\mathrm{A}_c = \sqrt{\mathrm{K}}\mathrm{A_{in}}$ and $\mathrm{A_{ac}} = \mathrm{i}\sqrt{1-\mathrm{K}}\mathrm{A_{in}}$, where K is the power splitting ratio of fiber coupler, the coupling ratio is therefore $100K : 100(1-K)$. The propagation of A_c and $\mathrm{A_{ac}}$ are separately simulated according to (1) with $\mathrm{g_0}= 0$, and they are changed to A'_c and A'_{ac} respectively after transmit though the passive fiber in the NOLM loop. Then the two counter-propagating fields are combined again at the fiber coupler to obtain the output light field $\mathrm{A}_{out} = \sqrt{K}A'_c + i\sqrt{1-K}\mathrm{A}'_{ac}$.

We solve (1) using the interaction picture method in the frequency domain, which is faster and more accurate than the common split-step Fourier method [30]. At the beginning of the simulation, random white noise is assumed at the starting position SMF1, and then propagated through each component in the cavity one by one. We repeat the oscillator round-trip iterations until the relative change of energy between 6 adjacent round-trips is below 10^{-5}, we determine that the laser has achieved a stable mode-locked regime and ended the simulation evolution process ahead of schedule.

A. Bandwidth of Filter

Assuming that the shape of the filter is an ideal Gaussian shape, we simulated the influence of bandwidth of the filter changed in the range between 2 nm to 10 nm (assuming the following fixed parameters: NOLM.L = 3.85 m, K = 30%). The general trends are shown in Fig. 2(a). In the range of bandwidth that we selected, only 4 nm can achieve 1∼6 pulses, 6nm/8nm/10 nm bandwidth can only realize stable single pulse mode-locking. And 2 nm bandwidth cannot get any stable mode-locked pulse, therefore it is not shown in the figure. The maximum single-pulse energy that can be supported by laser increases as the filter bandwidth increases, it is shown in Fig. 2(b). The filter bandwidth has a great influence on the number of pulses the mode-locked laser can output. Pulses in ANDi laser are highly chirped, spectral filtering with narrowband filter also results in reduced pulse widths, the shorter pulse will get higher peak power after amplification, then pulse splitting may occur due to the cavity pulse peak power clamping effect. When the bandwidth is large, only single pulse mode locking can be obtained. It can be inferred that the bandwidth of the filter selected in previous experiments is large [27], [31], so there was only single pulse mode-locking. When the bandwidth is small enough, multiple pulses can be realized, but if the bandwidth is too small, mode locking cannot be generated.

B. Length of NOLM Loop

We simulated the influence of length of NOLM loop in the range between 2 m to 5 m (assuming the following fixed parameters: Filter.BW = 4 nm, K = 30%). The general trends are shown in Fig. 3(a), all NOLM loop lengths enable achieve stable single-pulse and multi-pulse mode-locking states. With the increase of gss, the number of pulses will also increase, up to 6 mode-locked pulses can be obtained. In the case of multi-pulse mode locking, the multi-pulse mode locking can jump in N and N + 1 states by adjusting the gss (equivalent to adjusting the pump power) while keeping the structure of the mode-locking cavity unchanged.

Comparing the conditions of each group in Fig. 3(a), it can be found that when the length of NOLM loop is between 3∼4 m, the unstable region is relatively small, and the stable mode-locked region can be larger. In addition, as the length of NOLM loop increases, the maximum single-pulse energy that the mode-locked laser can support decreases, as shown in Fig. 3(b).

Fig. 4 shows the temporal waveforms of the fundamental mode-locking pulse with maximum energy at the output port of the laser and the entrance of the NOLM under different loop lengths. At the output port of the laser, we can see that as the

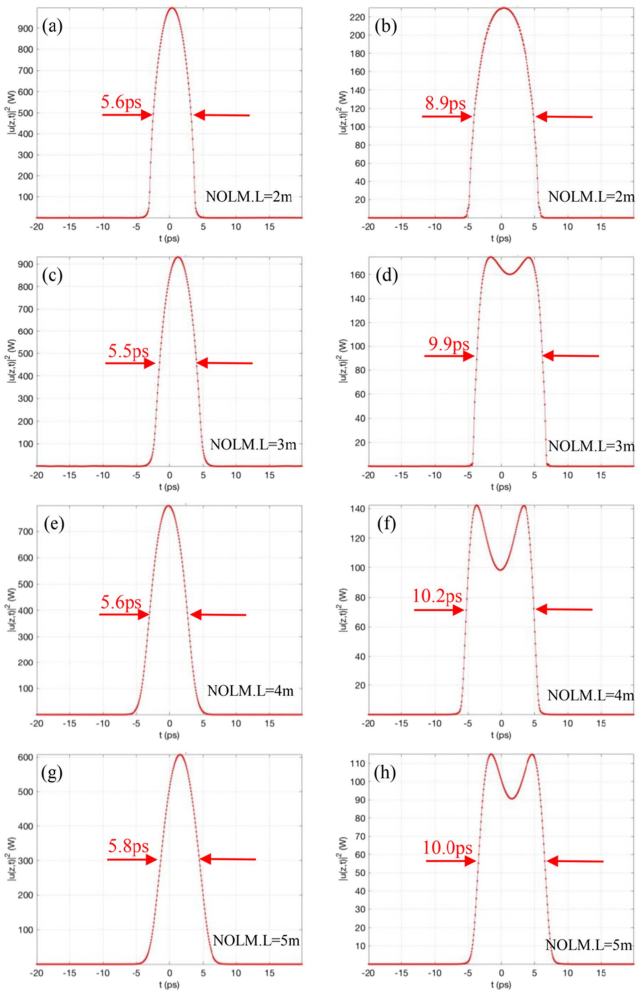

Fig. 4. The temporal waveforms at the entrance of NOLM and the output port of the laser. (a), (c), (e), (g) are the temporal waveforms at the entrance of NOLM respectively; (b), (d), (f), (h) are the temporal waveforms at the output port of the laser respectively.

length of NOLM loop increases, a more pronounced dip appears in the middle of the temporal pulse shape. At the entrance of NOLM, the temporal pulse width remains approximately constant in each case. As the length of NOLM loop increases, the peak power required to accumulate a certain amount of nonlinear phase delay decreases gradually. According to the above reasons, we can see that the maximum single pulse energy that the laser can support decreases with the increase of the NOLM loop length.

C. Coupler Power Splitting Ratio

The coupler power splitting ratio K mainly influences the light intensity difference between the clockwise and counterclockwise directions when the pulse enters the NOLM loop. A higher K results in a larger phase difference between the clockwise direction and counterclockwise direction.

We simulated the influence of the coupler power splitting ratio, which is changed in the range of 10% to 40% (assuming the following fixed parameters: Filter.BW = 4 nm, NOLM.L = 3.85m). The simulation results are shown in Fig. 5. When K = 10% or 20%, the laser does not achieve any stable single-pulse or multi-pulse mode locking, so they are not shown in the figure. Comparing the cases of K = 30% and K = 40%, it can be easily found that K = 30% can obtain mode-locking with various pulse numbers, while K = 40% can only obtain a single pulse. Although K = 30% is easier to enter the stable mode-locked state, the stable single-pulse mode-locking at K = 40% has a larger region and can support a higher maximum single pulse energy. Therefore, in practical applications, an appropriate K can be selected according to different requirements.

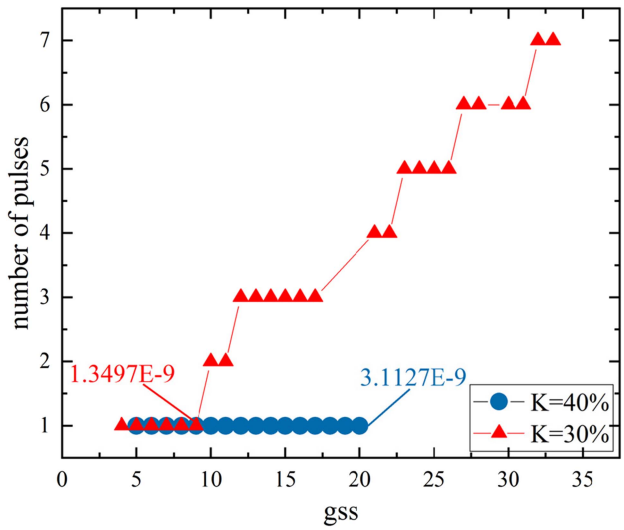

Fig. 5. Relationship between coupler power splitting ratio and number of pulses.

III. Experimental Setup and Measurements

The setup of the oscillator we used for experiments is basically the experimental realization of the design shown in Fig. 1. We chose the parameters according to the simulation results discussed above. The main loop of the laser contains a 1m long Yb-doped PM fiber (Nufern: PM-YSF-HI-HP). The filter used in [27] has a relatively broad pass-band with 11 nm full width at half-maximum (FWHM), while a narrow band-pass filter centered at 1030 nm with a 4 nm bandwidth is used in our case. A 40:60 fiber coupler extracts 40% of the intracavity power as output. The NOLM loop is made of a 30:70 fiber coupler and a piece of PM fiber. The passive optical fibers in the laser cavity are all Nufern PM 980-XP. The total length of the fiber laser cavity is around 15m. The temporal characteristics of the laser output were measured at different time scales. The pulse trains in a long temporal range (>100 ns) were measured by a 4 GHz oscilloscope (KEYSIGHT DSOS404A) together with a 2 GHz photodetector (Thorlabs DET025AFC/M). The pulse dynamics in the short temporal range (50 ps∼100 ns) were measured by a 22 GHz high-speed photodetector (EOT ET-3600) and a 13 GHz bandwidth sampling oscilloscope (KEYSIGHT DSA91304A). To better identify multiple pulses in the femtosecond to picosecond range (fs∼150ps), the laser output pulses were compressed by a grating pair, and the autocorrelation curves of the

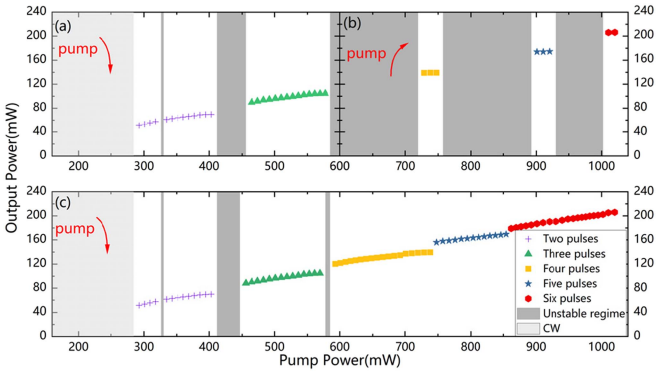

Fig. 6. Laser output power and pulse count with respect to pump power. Different symbols represent different numbers of pulses. (a) was measured by decreasing the pump power from 600 mW; (b) was measured by increasing the pump power from 600 mW; (c) was measured by decreasing the pump power from 1020 mW.

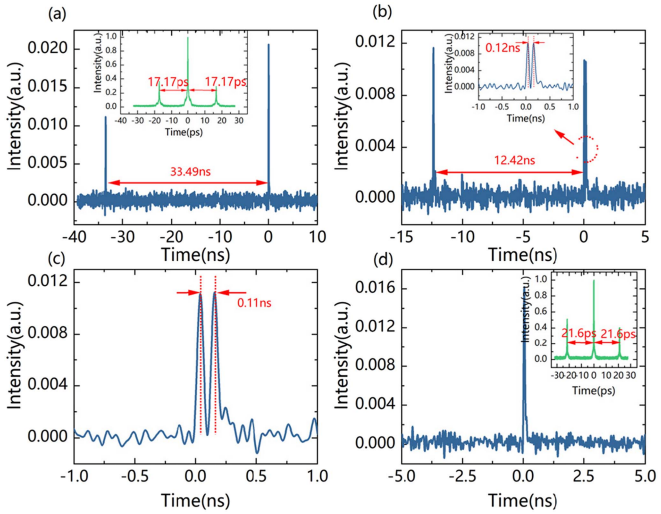

Fig. 7. Oscilloscope trace of laser output pulses in multi-pulse mode-locked state. Insets with green curve are autocorrelation traces of the compressed output pulses. (a) Pump power = 577 mW. (b) Pump power = 545 mW. (c) Pump power = 403 mW. (d) Pump power = 318 mW.

de-chirped pulses were measured by an intensity autocorrelator (Femtochrome FR-103XL).

A. Multi-Pulse Mode-Locking Results and Analyses

The laser can be triggered into an unstable pulse operation state at a pump power of 600 mW. Stable multi-pulse mode-locking states can be achieved by either decreasing or increasing the pump power. We have conducted a lot of tests, and some typical experimental results on the relationship between the number of stable mode-locked pulses per cavity round trip and the pump power are summarized in Fig. 6.

Fig. 6(a) is the results of tests, in which the laser first entered into an unstable pulse state at a pump power of 600 mW, and then we gradually reduced the LD drive current. In the test experiment related to Fig. 6(a), the laser started to operate in a stable three-pulse regime when the pump power was 577 mW. A single soliton and a soliton molecule 33.5 ns away from it coexisted in the cavity, as shown in Fig. 7(a). The separation time of two pulses in soliton molecule was so close that cannot be distinguished by the oscilloscope. The autocorrelation trace of the compressed laser pulse shown in the inset of Fig. 7(a) indicated that the pulse spacing is 17.2 ps. When the pump power was further reduced to 545 mW, the pulse interval in the soliton molecule increased to 120 ps, which can be identified by the oscilloscope, as shown in Fig. 7(b). The laser remained in the three-pulse mode-locked state until the pump power was lower than 474 mW, at this time, the laser was running in an unstable pulse regime. Further reducing the pump power to 403 mW, the isolated soliton in the three-pulse mode-locked state disappeared, and the laser began to enter a stable dual-pulse mode-locking state, as shown in Fig. 7(c). When the pump power gradually decreased from 403 mW to 334 mW, the pulse interval remained almost unchanged at 110 ps. The laser suddenly changed to an unstable pulse state at a pump power level of 326 mW, and then reverted to the double pulse mode-locked state when the pump power was 318 mW, the pulse interval at this time became 21.6 ps, as shown in Fig. 7(d). The laser was then maintained in a dual-pulse state until mode-locking broke

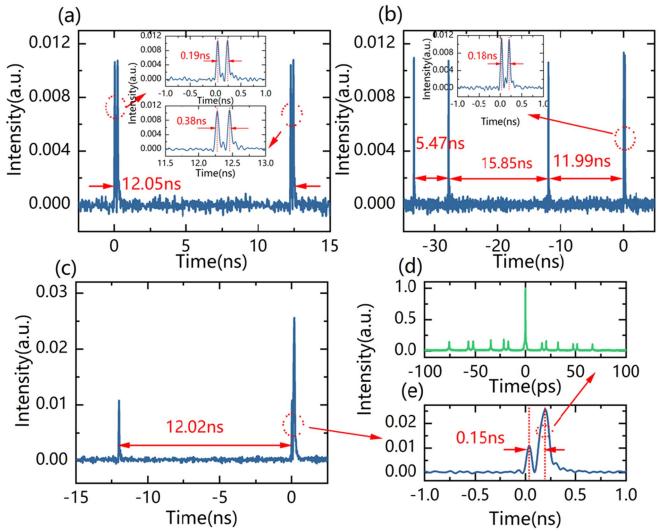

Fig. 8. Oscilloscope trace of laser output pulses in multi-pulse mode-locked state. (a) Pump power = 729 mW. (b) Pump power = 901 mW. (c) Pump power = 1010 mW. (d) Green curve are autocorrelation traces of the compressed output pulses.

when the pump power was below 293 mW, and the laser started to operate in a continuous wave mode.

In the test experiment related to Fig. 6(b), the laser also first triggered into an unstable pulse state at a pump power level of 600 mW, then we gradually increased the LD drive current. In Fig. 6(b), the laser entered into the four-pulse mode-locking state when the pump power was increased to 729 mW. 4 pulses are divided into two groups as shown in Fig. 8(a). The time separation between the two pulse pairs is 12 ns, while the temporal interval inside the pulse pair is 190 ps and 380 ps respectively. The laser operated in a 4-pulse mode-locking state until the pump power was greater than 748 mW and then entered into an unstable pulse

regime. The five-pulse mode-locking state occurred when the pump power reached 901 mW as shown in Fig. 8(b), and the laser remained in this state until the pump power exceeded 920 mW. When the pump power was further increased to 1010 mW, the laser re-entered into the stable multi-pulse mode-locking regime. The laser temporal waveform measured by the oscilloscope is shown in Fig. 8(c), where one pulse has high intensity and the other two pulses have lower intensity. Fig. 8(d) shows the autocorrelation trace of the compressed laser pulse. From this, we can infer that the high-intensity pulse is composed of four pulses with uneven spacing, which was so close that it cannot be distinguished by oscilloscope. Therefore, there are 6-pulse co-exist per round trip in the laser cavity. The laser cavity remained in this state when the pump power was increased to 1020 mW, which was the maximum output power of LD.

The mechanism of multiple pulse pattern formation and evolution observed in our experiment can be qualitatively explained as the cavity pulse peak power clamping effect [22], [26]. The transmission of NOLM is a sinusoidal function of the intensity-dependent phase delay with a period of 2π. By appropriately setting the phase delay, the NOLM can serve as a saturable absorber in favor of pulse formation and maintenance. Suppose a pulse has been circulating in the laser cavity, when the pump power is increased, the pulse peak power, as well as the nonlinear phase delay, is also increased. When the pulse peak power is higher than a center value, it can switch the cavity from positive feedback to negative feedback. In this case, background noise is more amplified than the intense pulse as the cavity feedback is still positive for the weak pulses. Further increasing the pump power then results in the formation of CW lasing from background noise. Due to the saturable absorption effect of NOLM, the modulation of the CW component is enhanced and causes the laser to operate in an unstable state. As the pump power increases further, the strongest background wave will be amplified and shaped into an additional pulse. The laser then returns to the stable mode-locking state with the number of pulses per cavity round trip increasing by 1. On the other hand, suppose the laser is initially in a stable multi-pulse mode-locked state, after the pump power decreases to a certain value, the laser will become unstable as the exact balance between gain and loss cannot be satisfied in the dissipative system. The CW component and pulses coexist in the cavity until the pump power is further decreased to support another stable mode-locking state, in which the number of pulses per cavity round trip is decreased by 1.

Fig. 6(a) and (b) also indicate that the area of the unstable pulse regime is smaller when the pump power is decreased than when the pump power is increased. To better verify this point, after the laser reached the mode-locked state of 6-pulse at the maximum pump power of 1020 mW, we gradually decreased the pump power level and recorded the relationship between the number of pulses and the pump power again, the result is shown in Fig. 6(c). As the pump power decreased gradually, the number of pulses per cavity round-trip decreased one by one. The evolution is different from that shown in Fig. 6(b), the transition among the states of a different number of pulses is possible without passing through the unstable pulse regime. Our experimental results are quite different from the results reported in [22], [25], [26], where the area of the unstable pulse regime is almost unchanged regardless of the pump power adjustment direction. We currently speculate that the linear cavity loss plays a key role in the different results. Our ANDi laser is mode-locked with an all-PM NOLM, which introduces a large amount of cavity loss for linear waves. Higher pump power is required to maintain the mode-locked state compared with [22], [25], [26]. As the pump power increases, the background noise also increases. Stronger background noise disturbances may lead to the instability of the original stable mode-locked state. Therefore, during the adjustment process of the pump power increase, the size of the unstable region is larger. On the contrary, when the pump power is gradually reduced, the intensity of the background noise is also reduced, and the disturbance received by the mode-locked pulses is reduced. Therefore, during the adjustment process of the pump power decrease, the laser is more likely to maintain a stable mode-locked state, and the area of the unstable region is reduced accordingly. The minimum pump power capable of supporting the N-pulse state is much lower than the pump power required for the N-pulse state to occur in the process of increasing the pump. Therefore, there was a strong hysteresis phenomenon that occurs as a function of pump power.

B. Fundamental Mode-Locking Results and Analyses

For many passively mode-locked fiber lasers, it is necessary to trigger mode-locking by turning up the pump power to a relatively high value. The laser works in a multi-pulse regime initially, then a single-pulse mode-locked state is obtained by decreasing the pump power. In our experiment, by gradually reducing the laser pump power, the number of pulses could be reduced one by one until two pulses coexist per cavity round trip in the laser. However, it failed to achieve a single-pulse mode-locked state by slightly decreasing the pump power, as shown in Fig. 6, when the pump power was reduced to about 280 mW, the laser lost mode-locking and turned to continuous-wave operation. To obtain single-pulse mode-locking, the laser enters into the dual-pulse mode-locking regime, and then directly decreased the pump power to a relatively low value rather than slowly reducing it. For example, by directly reducing the pump power from 300 mW to 217 mW, stable fundamental mode-locking was obtained with an output power of 32.8 mW. To the best of our knowledge, no relevant phenomenon has been reported in the literature. We speculate that this is due to the gain competition between the mode-locked pulse and the CW noise. When the pump power is reduced just below the threshold of two-pulse mode-locking, the intracavity gain cannot maintain stable operation of two mode-locked pulses. At this time, pulses and continuous wave noise will coexist in the cavity. Although the pump power can provide a gain much higher than that required for single-pulse mode-locking, due to the power clamping effect, the energy of a single pulse will not increase. On the contrary, the continuous optical noise will be sufficiently amplified to disturb the single-pulse state. The pulse cannot be maintained stably due to disturbance, and the laser cavity eventually loses the mode-locked state. On the other hand, if the pump power is sharply reduced to a lower value, the

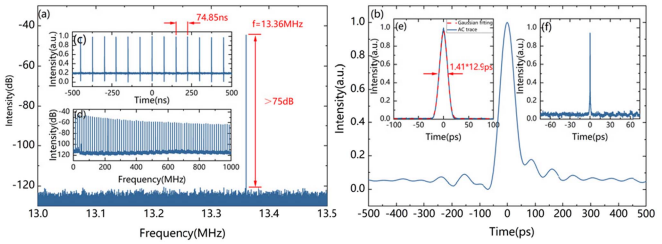

Fig. 9. (a) RF spectrum recorded at the fundamental frequency. Inset (c) The pulse train generated from the fiber oscillator. Inset (d) Harmonic RF spectrum. (b) Temporal waveform of the output pulse measured by a 22 GHz photodetector and a 13 GHz bandwidth oscillator. Inset (e) Autocorrelation trace of the chirped output pulse. Inset (f) Autocorrelation trace of the compressed pulse with a 160 ps long scanning range.

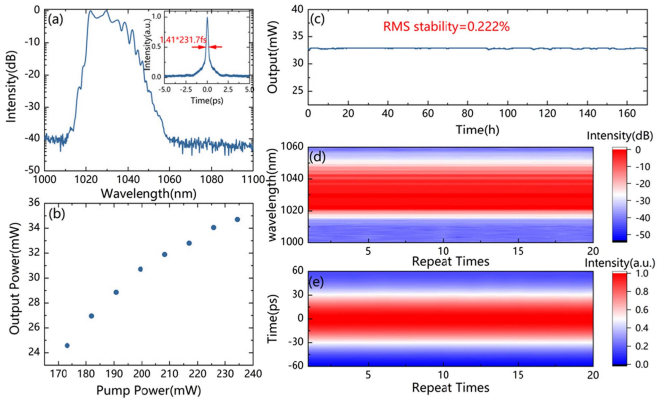

Fig. 10. (a) The pulse spectrum with a logarithmic scale and autocorrection trace of the de-chirped pulse output (inset). (b) Laser output power versus pump power when operated in a fundamental mode-locking state. (c) Laser output power stability in one week. (d) Spectra over 20 cycles of powering the laser on and off. (e) Pulse shape over 20 cycles of powering the laser on and off.

gain provided by the cavity will also be reduced to a lower level, then the continuous wave noise cannot be effectively amplified. For the two pulses that originally circulating in the cavity, the one with higher energy (for example, the pulse passing through the gain fiber first will obtain higher gain) will win the final gain competition, and the laser change to stable fundamental mode-locking state.

The fundamental repetition rate of the pulse train is measured to be 13.36 MHz, matching well with the ∼15 m cavity length and the measured pulse spacing of 74.85 ns as shown in the inset (c) of Fig. 9. The RF spectrum measured with 10 Hz resolution bandwidth and 500 KHz span gives a signal-to-noise ratio (SNR) exceeding ∼75 dB. The harmonic RF spectra was measured at a resolution of 100 Hz with a span of 1 GHz as shown in Fig. 9(d). The RF trace drops smoothly and no spectral modulation is observed, confirming the high amplitude stability of the fundamental mode-locking.

To further confirm that the laser operated in a single pulse state, we measured the temporal characteristics of the laser output at different time scales. First, a high-speed 22 GHz photodetector and a 13 GHz bandwidth oscillator were used to monitor the temporal waveform. The FWHM pulse duration is measured to be ∼60 ps. Although the oscilloscope trace cannot accurately represent the optical envelope due to limiting detector bandwidth, this measurement verifies that only one pulse exists in the time interval of 60 ps to 74 ns. The actual pulse duration of chirped laser output was measured directly by an intensity autocorrelator as shown in Fig. 9(e). The autocorrelation trace is close to the Gaussian shape with an FWHM duration of 18.2 ps, corresponding to a chirped pulse duration of 12.9 ps. Second, the chirped output pulses were compressed by a grating pair compressor, we optimized the grating separation to obtain the shortest pulse width. Fig. 9(f) presents the measured autocorrelation trace in 160 ps long scanning range, which checks out there are no satellite pulses on the shorter time scale (fs to 160 ps) and the laser does not work in a noise-like regime.

Assuming a Gaussian shape, the measured FWHM duration of the de-chirped pulse is 231.7 fs as shown in the inset of Fig. 10(a). The laser output spectrum was measured with an optical spectrum analyzer (YOKOGAWA AQ6370D). The spectrum is centered near 1030 nm with a broad bandwidth and steep edges, which are the typical characteristic of the ANDi lasers. The uneven modulation in the spectrum is due to the effect of self-phase modulation, high order dispersion, and the spectral filtering induced by NOLM. After the laser is operated in a single pulse regime, it can be steadily maintained in this state as the pump power varies from 173 mW to 234 mW. The relationship between the output power of the fundamental mode-locked laser and the pump power is shown in Fig. 10(b).

Long-term output power stability of the fundamental mode-locked laser at a pump power level of 217 mW was measured by a power meter (Ophir 3A). The laser works continuously for more than one week, without interruption of mode-locking. The fluctuation of the average power (32.85 mW) is only 0.222% (standard deviation divided by average) in 169 hours, as shown in Fig. 10(c). For single-pulse mode-locked operation, the characteristics of the laser have good repeatability. We turned the laser on and off 20 times, adjusted the pump power to 217 mW each time so that the laser can operate in the single pulse state, and then recorded the spectrum and the oscilloscope waveform. As shown in Fig. 10(d) and (e), each on-cycle resulted in generation of mode-locked laser pulse with almost constant parameters.

IV. Conclusion

We have demonstrated an all-PM Yb-doped fiber laser using NOLM. The influence of several cavity design parameters (bandwidth of filter, length of NOLM, and coupler power splitting ratio) on laser performance has been studied in numerical simulations. The effects of these parameters on the number of stable pulses and the maximum single pulse energy that can be supported by the laser are analyzed. Our numerical simulations provided a guideline for the parameter choice in the experiments.

In terms of experiments, we studied the formation of single-pulse and multi-pulse waveforms in an ANDi all-PM fiber figure-eight laser. DSs in the laser resonator could be created/annihilated one by one by gradually increasing/reducing the pump power provided that there are more than two pulses in the resonator. Up to 6 DSs coexist per cavity round trip

was demonstrated at maximum pump power. There was strong pump hysteresis phenomenon. The transition between the states with N and N + 1 pulse per round trip is only possible by passing through an area of unstable pulse regime when the pump power is increasing. When the pump power is reduced, intervals of the unstable pulse operation shrink or disappear altogether. To obtain stable fundamental mode-locking, the pump power should be abruptly reduced to a relatively low value rather than slowly reducing it. Once the laser enters into a single pulse mode-locking state, it shows excellent stability and good repeatability.

REFERENCES

[1] A. S. Mayer et al., "Flexible all-PM NALM Yb: Fiber laser design for frequency comb applications: Operation regimes and their noise properties," *Opt. Exp.*, vol. 28, no. 13, pp. 18946–18968, 2020.

[2] A. Ancona, F. Röser, K. Rademaker, J. Limpert, and A. Tünnermann, "High speed laser drilling of metals using a high repetition rate, high average power ultrafast fiber CPA system," *Opt. Exp.*, vol. 16, no. 12, pp. 8958–8968, 2008.

[3] S. Wang, Y. Li, Y. Chen, Y. Gao, Z. Zhang, and A. Wang, "Femtosecond all-polarization-maintaining Nd fiber laser at 920 nm mode locked by a biased NALM," *Opt. Exp.*, vol. 29, no. 23, pp. 38199–38205, 2021.

[4] A. Chong, W. H. Renninger, and F. W. Wise, "Environmentally stable all-normal-dispersion femtosecond fiber laser," *Opt. Lett.*, vol. 33, no. 10, pp. 1071–1073, 2008.

[5] A. Chong, W. H. Renninger, and F. W. Wise, "All-normal-dispersion femtosecond fiber laser with pulse energy above 20nJ," *Opt. Lett.*, vol. 32, no. 16, pp. 2408–2410, 2007.

[6] X. Fan, S. Wang, Y. Wang, D. Shen, D. Tang, and L. Zhao, "Pump hysteresis and bistability of dissipative solitons in all-normal-dispersion fiber lasers," *Appl. Opt.*, vol. 54, no. 12, pp. 3774–3779, 2015.

[7] C. Aguergaray, N. G. R. Broderick, M. Erkintalo, J. S. Y. Chen, and V. Kruglov, "Mode-locked femtosecond all-normal all-PM Yb-doped fiber laser using a nonlinear amplifying loop mirror," *Opt. Exp.*, vol. 20, no. 10, pp. 10545–10551, 2012.

[8] C. Aguergaray, R. Hawker, A. Runge, M. Erkintalo, and N. Broderick, "120 fs, 4.2 nJ pulses from an all-normal-dispersion, polarization-maintaining, fiber laser," *Appl. Phys. Lett.*, vol. 103, no. 12, pp. 3550–3554, 2013.

[9] A. F. J. Runge, C. Aguergaray, R. Provo, M. Erkintalo, and N. G. R. Broderick, "All-normal dispersion fiber lasers mode-locked with a nonlinear amplifying loop mirror," *Opt. Fiber Technol.*, vol. 20, no. 6, pp. 657–665, 2014.

[10] L. Gui et al., "Soliton molecules and multisoliton states in ultrafast fibre lasers: Intrinsic complexes in dissipative systems," *Appl. Sci.*, vol. 8, no. 2, 2018, Art. no. 201.

[11] F. Amrani, A. Haboucha, M. Salhi, H. Leblond, A. Komarov, and F. Sanchez, "Dissipative solitons compounds in a fiber laser. Analogy with the states of the matter," *Appl. Phys. B*, vol. 99, no. 1, pp. 107–114, 2010.

[12] F. Amrani, M. Salhi, H. Leblond, and F. Sanchez, "Characterization of soliton compounds in a passively mode-locked high power fiber laser," *Opt. Commun.*, vol. 283, no. 24, pp. 5224–5230, 2010.

[13] F. Amrani et al., "Passively mode-locked erbium-doped double-clad fiber laser operating at the 322nd harmonic," *Opt. Lett.*, vol. 34, no. 14, pp. 2120–2122, 2009.

[14] S. Chouli and P. Grelu, "Rains of solitons in a fiber laser," *Opt. Exp.*, vol. 17, no. 14, pp. 11776–11781, 2009.

[15] C. Bao, X. Xiao, and C. Yang, "Soliton rains in a normal dispersion fiber laser with dual-filter," *Opt. Lett.*, vol. 38, no. 11, pp. 1875–1877, 2013.

[16] S. Chouli and P. Grelu, "Soliton rains in a fiber laser: An experimental study," *Phys. Rev. A*, vol. 81, no. 6, 2010, Art. no. 063829.

[17] A. Komarov, K. Komarov, and F. Sanchez, "Quantization of binding energy of structural solitons in passive mode-locked fiber lasers," *Phys. Rev. A*, vol. 79, no. 3, 2009, Art. no. 033807.

[18] M. Stratmann, T. Pagel, and F. Mitschke, "Experimental observation of temporal soliton molecules," *Phys. Rev. Lett.*, vol. 95, no. 14, 2005, Art. no. 143902.

[19] L. Yun and X. Liu, "Generation and propagation of bound-state pulses in a passively mode-locked figure-eight laser," *IEEE Photon. J.*, vol. 4, no. 2, pp. 512–519, Apr. 2012.

[20] M. Long, H. Deng, and H. Zhang, "Development of multiple pulse picosecond laser with 1 kHz repetition rate and its application in space debris laser ranging," *Acta Optica Sinica*, vol. 41, no. 6, 2021, Art. no. 0614001.

[21] A. Nebel et al., "Generation of tailored picosecond-pulse-trains for micromachining," *Proc. SPIE*, vol. 6108, 2006, pp. 226–233.

[22] D. Tang, L.-M. Zhao, B. Zhao, and A. Liu, "Mechanism of multisoliton formation and soliton energy quantization in passively mode-locked fiber lasers," *Phys. Rev. A*, vol. 72, no. 4, 2005, Art. no. 043816.

[23] Y. Wang et al., "Nonlinear Fourier transform enabled eigenvalue spectrum investigation for fiber laser radiation," *Photon. Res.*, vol. 9, no. 8, pp. 1531–1539, 2021.

[24] Y. Wang et al., "Soliton distillation of pulses from a fiber laser," *J. Lightw. Technol.*, vol. 39, no. 8, pp. 2542–2546, Apr. 2021.

[25] A. Haboucha, A. Komarov, H. Leblond, F. Sanchez, and G. Martel, "Mechanism of multiple pulse formation in the normal dispersion regime of passively mode-locked fiber ring lasers," *Opt. Fiber Technol.*, vol. 14, no. 4, pp. 262–267, 2008.

[26] X. Liu, "Hysteresis phenomena and multipulse formation of a dissipative system in a passively mode-locked fiber laser," *Phys. Rev. A*, vol. 81, no. 2, 2010, Art. no. 023811.

[27] J. Szczepanek, T. M. Kardaś, M. Michalska, C. Radzewicz, and Y. Stepanenko, "Simple all-PM-fiber laser mode-locked with a nonlinear loop mirror," *Opt. Lett.,* vol. 40, no. 15, pp. 3500–3503, 2015.

[28] J.-H. Cai, H. Chen, S.-P. Chen, and J. Hou, "State distributions in two-dimensional parameter spaces of a nonlinear optical loop mirror-based, mode-locked, all-normal-dispersion fiber laser," *Opt. Exp.*, vol. 25, no. 4, pp. 4414–4428, 2017.

[29] M. Pielach, B. Piechal, J. Szczepanek, P. Kabaciński, and Y. Stepanenko, "Energy scaling of an ultrafast all-PM-fiber laser oscillator," *IEEE Access*, vol. 8, pp. 145087–145091, 2020.

[30] J. Hult, "A fourth-order runge–kutta in the interaction picture method for simulating supercontinuum generation in optical fibers," *J. Lightw. Technol.*, vol. 25, no. 12, pp. 3770–3775, Dec. 2007.

[31] L. M. Zhao, A. C. Bartnik, Q. Q. Tai, and F. W. Wise, "Generation of 8 nJ pulses from a dissipative-soliton fiber laser with a nonlinear optical loop mirror," *Opt. Lett.*, vol. 38, no. 11, pp. 1942–1944, 2013.